Topology optimization for submerged buoyant structures

Picelli, R. ; van Dijk, R.; Vicente, W.M.; Pavanello, R.; Langelaar, M.; van Keulen, F.

DOI
10.1080/0305215X.2016.1164147

Publication date
2017

Document Version
Accepted author manuscript

Published in
Engineering Optimization

Citation (APA)
Picelli, R., van Dijk, R., Vicente, W. M., Pavanello, R., Langelaar, M., & van Keulen, F. (2017). Topology optimization for submerged buoyant structures. *Engineering Optimization*, *49*(1), 1-21. https://doi.org/10.1080/0305215X.2016.1164147

RESEARCH ARTICLE

Topology Optimization for Submerged Buoyant Structures

R. Picelli[†*], R. van Dijk[‡], W.M. Vicente[†], R. Pavanello[†],M. Langelaar[§] and F. van Keulen[§]

[†]*Department of Computational Mechanics, Faculty of Mechanical Engineering, University of Campinas, Rua Mendeleyev 200, 13083-860, Campinas, Brazil*;

[‡]*van Dijk FEM engineering B.V., Simonsstraat 14, 2628 TH, Delft, The Netherlands*;

[§]*Structural and Optimization Mechanics, Faculty of Mechanical, Maritime and Materials Engineering, Delft University of Technology, Mekelweg 2, 2628 CD, Delft, The Netherlands*;

(*v1.0 released June 2014*)

This paper presents an evolutionary structural topology optimization method for design of completely submerged buoyant modules with design-dependent fluid pressure loading. This type of structure is used to support offshore rig installation and pipeline transportation in all water depths. The proposed optimization method seeks to identify the buoy design that has the highest stiffness, allowing it to withstand deepwater pressure, uses the least material and has a minimum prescribed buoyancy. Laplace's equation is used to simulate an underwater fluid pressure, and a polymer buoyancy module is considered to be linearly elastic. Both domains are solved with the finite element method. Using an extended bi-directional evolutionary structural optimization (BESO) method, the design-dependent pressure loads are modeled in a straightforward manner without any need for pressure surface parametrization. A new buoyancy inequality constraint sets a minimum required buoyancy effect, measured by the joint volume of the structure and its interior voids. Solid elements with low strain energy are iteratively removed from the initial design domain until a certain prescribed volume fraction. A test case is described to validate the optimization problem, and a buoy design problem is used to explore the features of the proposed method.

Keywords: Topology Optimization; BESO Method; Buoyancy; Buoyant Structures; Subsea Buoyancy Modules;

1. Introduction

Structural topology optimization (Bendsoe and Kikuchi 1988; Bendsoe and Sigmund 2003) has been used extensively in structural design problems, especially in the aerospace and automotive industries. Over the last decade considerable effort has been made to extend the methods used in topology optimization to different problems, such as those involving different objective functions, constraints and multiphysics problems (Yoon, Jensen and Sigmund 2007; Duhring, Jensen and Sigmund 2008; Silva and Pavanello 2010; van Dijk et al. 2013). Here, it is proposed the use of topology optimization in offshore structural engineering, specifically in the design of completely submerged (subsea) buoyancy modules to support oil pipelines. Subsea buoyancy modules provide buoyancy forces for offshore pipelines (flexible risers, cables and umbilicals) to hold them in specific

*Corresponding author. Email: PicelliR@cardiff.ac.uk

geometric configurations other than the natural self-weight catenary riser shape, as seen in Figure 1 (Saito et al. 2011). Buoyancy also reduces the overall weight of the pipeline system, increasing buckling load values. Deepwater buoyancy modules of this type are usually made from polymers and may be used at water depths of up to 2000 m.

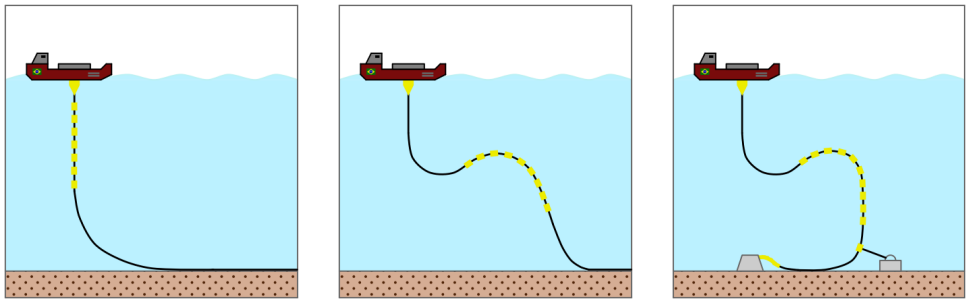

Catenary riser Lazy wave Pliant wave

Figure 1.: Examples of geometric configurations of subsea oil pipelines supported by buoyancy modules, represented as bullets in the illustrations. Buoyancy modules provide upward forces which counteracts the pipeline weight, holding the pipelines in the desired configurations.

To design subsea polymer buoys with topology optimization, buoyancy effects and design-dependent underwater pressure loads must be considered. Topology optimization considering interior voids has already been explored, as in the paper by Clausen, Aage and Sigmund (2014), but buoyancy has not been considered. To the best of the authors' knowledge, the present paper is the first to take buoyancy effects into account in topology optimization. Design-dependent pressure loads have proved to be a challenging topic for topology optimization (Sigmund and Clausen 2007) and are still the subject of research (Deaton and Grandhi 2014; Xia, Wang and Shi 2015).

The difficulties in optimizing structures subjected to pressure loads arise because of the variation in the location, direction and magnitude of the loads during the optimization procedure. This variation requires additional modeling techniques when the traditional density-based topology optimization methods are applied in such problems. For instance, in the SIMP model (Bendsoe and Sigmund 2003), the pressure-loaded surfaces are not explicitly defined because of the existence of intermediate density (gray scale) elements (Hammer and Olhoff 2000). The main efforts to solve pressure-load problems in topology optimization have used pressure surface parametrization schemes (Hammer and Olhoff 2000; Du and Olhoff 2004a; Lee and Martins 2012; Zheng, Chang and Gea 2009; Zhang, Liu and Zhang 2010) and multiphysics approaches (Chen, Silva and Kikuchi 2001; Bourdin and Chambolle 2003; Sigmund and Clausen 2007; Bruggi and Cinquini 2009). These works showed that pressure loading problems can be efficiently solved with density-based topology optimization by using different pressure boundaries modeling techniques. The idea of using mixed element formulations by Sigmund and Clausen (2007) could be further applied in a range of different multiphysics problems (Yoon, Jensen and Sigmund 2007; Yoon and Sigmund 2008; Yoon 2010).

On the other hand, Picelli, Vicente and Pavanello (2015) proposed an extended BESO method for use in hydrostatic fluid-loaded structural design problems using a partially coupled fluid-structure formulation. Because of the discrete nature of the BESO method, no intermediate density elements are allowed during the optimization and the problem is solved without any need for pressure load surface parametrization schemes. In comparison with the SIMP model, the BESO scheme can be used with staggered analysis and separate domains, which can be handy for its association with commercial finite element codes

and the use of classical formulations. However, the evolutionary methods still lack of procedures in handling multiple linear and nonlinear constraints, while this is simpler to be considered with the density-based methods.

The idea by Picelli, Vicente and Pavanello (2015) was extended to acoustic-structure interaction problems, as shown by Vicente et al. (2015) and Picelli et al. (2015a). This evidences the recent uses of the BESO method on multiphysics problems (Picelli et al. 2015b; Picelli 2015). The discrete nature of these methods are also recently explored in multiscale problems (Zuo et al. 2013; Xia and Breitkopf 2014; Huang et al. 2015; Xia and Breitkopf 2015; Vicente et al. 2015). Similar approaches can also be adopted by other topology optimization methods with explicit boundaries definition, such as level set based methods (Luo et al. 2012; Shu, Wang and Ma 2014; Xia, Wang and Shi 2015).

A global outline of the present approach is as follows. To handle pressure loads, the fluid-structure BESO method described by Picelli, Vicente and Pavanello (2015) is used. This approach substitutes some of the void elements with hydrostatic fluid ones that can model the pressure field. Laplace's equation is used to model the fluid domain, allowing the existence of constant and non-constant pressure fields at wet fluid-structure interfaces. The use of surface coupling matrices turns out the problem handy for the discrete topology optimization scheme by transfering pressure loads automatically to the structural analysis whatsoever is the structural topology. Herein, buoyancy requirements are introduced as an inequality constraint in the optimization problem. According to Archimedes' principle, the buoyancy force is equivalent to the weight of the fluid displaced by the submerged structure and can be expressed as:

$$\mathbf{F}_B = -\rho_f V_f \mathbf{g}_a, \tag{1}$$

where $\mathbf{F}_B$ is the buoyancy force acting on the structure, ρ_f is the mass density of the fluid, V_f the volume of the displaced fluid and $\mathbf{g}_a$ the vector of the gravitational acceleration. The force $\mathbf{F}_B$ is balanced by the weight $\mathbf{W}_s$ of the structure, expressed as:

$$\mathbf{W}_s = m_s \mathbf{g}_a, \tag{2}$$

where m_s is the mass of the structure, implying in a resulting force

$$\mathbf{F}_{resulting} = \mathbf{F}_B + \mathbf{W}_s. \tag{3}$$

As the mass of the structure is a constraint in the proposed optimization method, $\mathbf{W}_s$ is constant and the only variable in the force diagram is $\mathbf{F}_B$, which depends exclusively on V_f, since ρ_f and g_a are also constant. The volume V_f of the displaced fluid is equivalent to the sum of the volumes of the structural material and the buoy's interior voids. Thus, in order to guarantee higher buoyancy, the entire buoy volume (including structure and interior voids) must be as big as possible, implying in a positive $\mathbf{F}_{resulting}$. In this work it is assumed that the buoyancy modules must withstand the underwater surrounding pressure and exhibit minimal deformation so that they maintain the correct displaced volume. Hence, the final goal of the optimization problem is to design a structure as stiff as possible that can handle design-dependent underwater pressure loads and has high buoyancy (displaced fluid volume).

This article is organized as follows: Section 2 introduces the governing equations and the finite element model for the fluid-structure system. In Section 3, the topology optimization problem and sensitivity analysis are described. Section 4 discusses implementation issues and the steps in the fluid-structure BESO method. Section 5 presents the discussion and the numerical results obtained using the proposed methodology. Section 6 presents final conclusions.

2. Fluid-structure model: governing equations and finite element discretization

It is considered the static analysis of completely submerged flexible structures floating in an incompressible fluid domain. The use of subsea buoyancy modules in deepwater conditions implies high pressures in the fluid domain. Because of the depth at which the modules are operating, these pressures can be considered constant in this case.

The governing equation considering a homogeneous, inviscid, irrotational fluid domain Ω_f can be described by Laplace's equation

$$\nabla^2 P_f = 0 \qquad \text{in } \Omega_f, \tag{4}$$

where P_f is the fluid pressure (Morand and Ohayon 1995). A Dirichlet boundary condition (b.c.) boundary condition $P_f = P_0$ is applied on the particular portion S_p of the fluid boundary, as illustrated in Figure 2. The term P_0 is the imposed deepwater pressure value and must be different than zero.

Neglecting body forces, a linear structural static analysis is governed by

$$\nabla \cdot \boldsymbol{\sigma}_s(\mathbf{u}) = 0 \qquad \text{in } \Omega_s, \tag{5}$$

where $\nabla \cdot \boldsymbol{\sigma}_s(\mathbf{u})$ is the divergence of the Cauchy stress tensor and $\mathbf{u}$ is the displacement field on the solid domain Ω_s. Dirichlet boundary condition is applied to the solid boundaries S_u as $\mathbf{u} = 0$. A void domain Ω_v can also exist inside the solid domain.

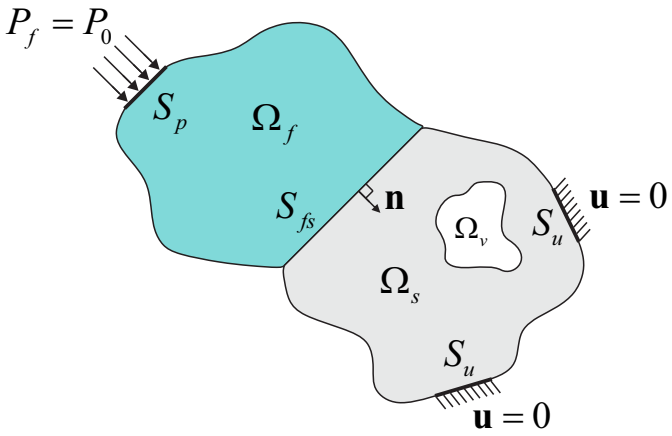

Figure 2.: The solid (Ω_s), fluid (Ω_f) and void (Ω_v) domains and boundary conditions. Pressure P_0 is imposed on the portion S_p of the fluid boundary. Fluid pressure loads acts on the structure through the fluid-structure interface S_{fs}.

The normal vector $\mathbf{n}$ (see Figure 2) can be used in order to guarantee the equilibrium condition between fluid pressures and structural tractions on the interface S_{fs} as follows:

$$\boldsymbol{\sigma}_s \mathbf{n} = -P_f \mathbf{n} \qquad \text{on } S_{fs}. \tag{6}$$

This equation ensures the continuity in pressure on the the interface S_{fs}, which indicates the pressure forces $\mathbf{f}_{fs} = P_f \mathbf{n}$ exerted by the fluid on the structure.

Using an approximation based on the finite element method (FEM), the force acting

on the structure provided by the fluid pressure can be calculated as

$$\mathbf{f}_{fs} = \int_{S_{fs}} \mathbf{N}_s^T \mathbf{n} \mathbf{N}_f dS_{fs} \mathbf{P}_f = \mathbf{L}_{fs} \mathbf{P}_f, \tag{7}$$

where $\mathbf{P}_f$ is the vector of nodal pressures, $\mathbf{n}$ is the normal vector inwards the structural domain and $\mathbf{N}_s$ and $\mathbf{N}_f$ contains the finite element shape functions for the interface. The matrix $\mathbf{L}_{fs}$ is the coupling matrix (Morand and Ohayon 1995; Axisa and Antunes 2007).

Thus, in the context of the finite element approximation, and assuming no external loads are applied, the hydroelastic equilibrium problem can be described by a non-symmetric system of equations

$$\begin{bmatrix} \mathbf{K}_s & -\mathbf{L}_{fs} \\ \mathbf{0} & \mathbf{K}_f \end{bmatrix} \begin{Bmatrix} \mathbf{u}_s \\ \mathbf{P}_f \end{Bmatrix} = \begin{Bmatrix} \mathbf{0} \\ \mathbf{0} \end{Bmatrix}, \tag{8}$$

where $\mathbf{u}_s$ is the vector of structural displacements and $\mathbf{K}_s$ and $\mathbf{K}_f$ are the stiffness matrices of the structural and fluid domains, respectively.

In this one-way coupled multiphysics model, the fluid analysis provides pressure loads to the structural analysis through the application of the coupling matrices. In this case, the fluid pressure field can actually be solved separately. However, for the sake of generality, by imposing proper boundary conditions and solving Equation 8, both fluid and structure responses can be obtained simultaneously for any discretized fluid-structure configuration. This turns to be handy for the iterative procedures of topology optimization. Furthermore, this methodology can be extended to different design-dependent physics problems, where fully coupled equations might exist (Vicente et al. 2015; Picelli et al. 2015a).

3. Problem formulation and sensitivity analysis

3.1 *Topology optimization problem*

The buoy design problems considered in this work involve minimizing the mean compliance of structures under design-dependent pressure loads while satisfying volume and buoyancy constraints. The goal is to find how a given amount of solid material should be distributed to ensure that the structure has maximum stiffness (or minimum compliance C) and a prescribed buoyancy. The corresponding evolutionary topology optimization problem can be formulated as:

$$\begin{aligned} \min_{x_i}: \quad & C(x_i) = \tfrac{1}{2} \mathbf{u}_s^T \mathbf{K}_s \mathbf{u}_s, \\ \text{subject to:} \quad & \begin{bmatrix} \mathbf{K}_s & -\mathbf{L}_{fs} \\ \mathbf{0} & \mathbf{K}_f \end{bmatrix} \begin{Bmatrix} \mathbf{u}_s \\ \mathbf{P}_f \end{Bmatrix} = \begin{Bmatrix} \mathbf{0} \\ \mathbf{0} \end{Bmatrix} \text{ and b.c.}, \\ & g = 1 - \tfrac{B}{B_{lim}} \leq 0, \\ & h = V(x_i)/V_0 = V_s, \\ & x_i = [0,1], \end{aligned} \tag{9}$$

where C is the structural mean compliance (external work), the inverse measure of the overall stiffness of the structure or its flexibility, B_{lim} is the minimum required buoyancy volume (displaced fluid area for 2D cases), B is the buoyancy volume of the current structural design, V_0 is the full design domain volume, V_s is the prescribed final solid volume fraction and x_i represents the discrete design variables, 1 being a solid element and 0 a void. The extended BESO method substitutes some of the void elements by incompressible fluid ones capable of modelling the pressure field. First, the standard BESO update scheme is used to set a 0/1 design. Then, the fluid region is updated considering their neighbouring elements. For instance, new fluid elements should be placed only besides fluid neighbour elements, as illustrated in Figure 3. Fluid elements which appear inside the design domain are considered equivalent to a void design variable ($x_i = 0$) in the optimization procedure, i.e., in the sensitivity analysis and in the 0/1 update scheme. However, they are fluid elements in the finite element analysis.

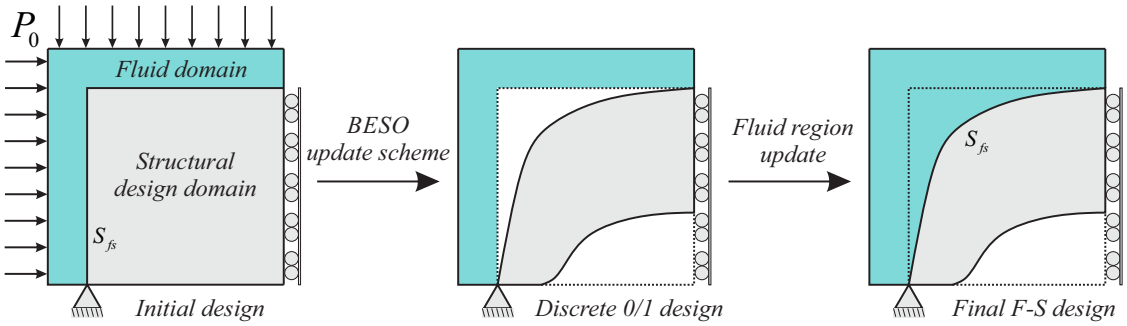

Figure 3.: Optimization step: fluid region update as a new operation in each iteration of the BESO method procedure.

The inequality constraint g sets a threshold for the required buoyancy volume and the equality constraint h sets the amount of solid material to be used with respect to the volume of the design domain. The constraint g is considered to be active when B, measured by the joint volume of structural and void elements, is equal as the prescribed buoyancy volume B_{lim}. The final solution do not need to present an active g, since $B > B_{lim}$ is also in the feasible solution region and it g is inactive in this case. The constraint h must be active in the final solution, ensuring the solution to present a final volume fraction equal to V_s.

To enable the procedures in the standard evolutionary method to be used, the previous problem statement is modified so that it can be solved in a penalty form (Luenberger and Ye 2008). Thus, the topology optimization problem becomes:

$$\begin{aligned} \min_{x_i}: \quad & f(x_i) = \tfrac{1}{2}\mathbf{u}_s^T \mathbf{K}_s \mathbf{u}_s + p\max(0,g), \\ \text{subject to:} \quad & \begin{bmatrix} \mathbf{K}_s & -\mathbf{L}_{fs} \\ \mathbf{0} & \mathbf{K}_f \end{bmatrix} \begin{Bmatrix} \mathbf{u}_s \\ \mathbf{P}_f \end{Bmatrix} = \begin{Bmatrix} \mathbf{0} \\ \mathbf{0} \end{Bmatrix} \text{ and b.c.}, \\ & h = V(x_i)/V_0 = V_s, \\ & x_i = [0,1], \end{aligned} \tag{10}$$

where p is an arbitrary penalty factor. When B is lower than B_{lim}, g is greater than 0 and is added to the objective function $f(x_i)$. This behavior is then discouraged by a high

penalty factor.

3.2 *Sensitivity analysis*

Starting from a full design domain (or initial solution), the BESO method slowly removes elements and reduces the solid volume fraction towards V_s. Void elements near high-stressed regions can return to the solid (Xie and Steven 1993; Huang and Xie 2010). A sensitivity analysis is needed to determine the efficiency of each element in the structural performance and decide which element should be eliminated or returned to solid. The sensitivity of $f(x_i)$ with respect to x_i is:

$$\frac{\partial f(x_i)}{\partial x_i} = \alpha_{Ci} + p\alpha_{Bi}, \tag{11}$$

where α_C and α_B correspond to the derivatives of the compliance and buoyancy objective functions, respectively. The derivative of the compliance is

$$\alpha_{Ci} = \frac{\partial C}{\partial x_i} = \mathbf{u}_s^T \mathbf{K}_s \frac{\partial \mathbf{u}_s}{\partial x_i} + \frac{1}{2}\mathbf{u}_s^T \frac{\partial \mathbf{K}_s}{\partial x_i}\mathbf{u}_s. \tag{12}$$

This compliance derivative is exactly the same as developed by Picelli, Vicente and Pavanello (2015) and detailed description of it can be found in the reference paper or in Picelli (2015). By deriving the equilibrium to find the unknown $\partial \mathbf{u}_s/\partial x_i$ and reorganizing the expression, the sensitivity of the compliance part is

$$\alpha_{Ci} = \mathbf{u}_s^T \frac{\partial \mathbf{L}_{fs}}{\partial x_i}\mathbf{P}_f - \frac{1}{2}\mathbf{u}_s^T \frac{\partial \mathbf{K}_s}{\partial x_i}\mathbf{u}_s. \tag{13}$$

The derivative of the buoyancy can be expressed as

$$\alpha_{Bi} = \frac{\partial g}{\partial x_i} = \frac{\partial(1 - \frac{B}{B_{lim}})}{\partial x_i} = -\frac{1}{B_{lim}}\frac{\partial B}{\partial x_i}. \tag{14}$$

The derivatives must be then evaluated locally at the element level, generating a sensitivity number α_i for each element represented by both compliance (α_{Ci}) and buoyancy (α_{Bi}) element sensitivities.

The version of the BESO method described here is developed using a hard-kill technique, where the densign variables of the void elements are set to zero, as proposed by Huang and Xie (2007). A material interpolation scheme similar to the SIMP method can also be used to set a very small density (design variable) for the void elements in a soft-kill evolutionary procedure described by Huang and Xie (2009). When used with a mesh-independency filter, both hard-kill and soft-kill approaches present similar results for structural design and can be used in a similar manner, as shown in Huang and Xie (2009).

In the present paper, the hard-kill BESO method is chosen to allow void elements to be completely replaced by fluid ones and to ensure better control of the buoyancy area[1]. In this approach, no material interpolation functions or design variables with very small values appear in the element modeling and the sensitivities cannot be calculated with continuous functions in the manner it is carried out by the SIMP approach. Therefore,

[1]The term "buoyancy area" is used to refer to the cross sectional area of the buoy.

an approximation based on a single step finite difference can be carried out for the hard-kill sensitivities, considering the structural configuration before and after an element removal (Huang and Xie 2010). The derivative of the global structural stiffness matrix with respect to the design variable of the ith element can be then expressed as

$$\frac{\partial \mathbf{K}_s}{\partial x_i} \approx \Delta \mathbf{K}_s(x_i) = \mathbf{K}_s^i. \tag{15}$$

The derivative of the coupling matrix $\partial \mathbf{L}_{fs}/\partial x_i$ indicates the change in the coupling condition when the ith element is removed. This change can be predicted by a finite difference with step equivalent as the system configuration before and after the element removal. Thus,

$$\frac{\partial \mathbf{L}_{fs}}{\partial x_i} \approx \Delta \mathbf{L}_{fs}(x_i) = \left(\mathbf{L}_{fs}^* - \mathbf{L}_{fs}\right)^i = \mathbf{L}_c^i, \tag{16}$$

where $\mathbf{L}_{fs}$ is the coupling matrix before the element is removed and $\mathbf{L}_{fs}^*$ is the final coupling matrix after the element is removed, resulting in a matrix assembled according to this change, as detailed by Picelli, Vicente and Pavanello (2015).

To find α_{Bi}, the derivative $\partial B/\partial x_i$ must be calculated. This derivative represents the change in the total buoyancy volume B when element x_i is removed. The absolute change in B can be approximated as

$$\left(\frac{\partial B}{\partial x_i}\right)^i \approx |\Delta B(x_i)| = |(B^* - B)^i| = (A_i)^{fs}, \tag{17}$$

where B^* is the buoyancy volume after removal of the ith element, and the superscript fs indicates that the term is valid only for elements at the fluid-structure interface. Removal of elements in the interior of the structure does not cause any change in B. For 2D cases, solid elements at the fluid-structure boundaries cause a change equivalent to the area A_i of the element. In these cases, the derivative of the buoyancy objective function is a constant valid only for solid elements at the fluid-structure interface. For all other elements, the sensitivity value is 0. Thus, returning to Equation 14, α_{Bi} can be expressed as

$$\alpha_{Bi} = \frac{\partial g}{\partial x_i} \approx -\frac{1}{B_{lim}} (A_i)^{fs}. \tag{18}$$

Finally, the sensitivity numbers for the present buoyancy-module design are

$$\alpha_i = -\frac{\partial f(x_i)}{\partial x_i} = \begin{cases} \frac{1}{2}\mathbf{u}_i^T \mathbf{K}_s^i \mathbf{u}_i - \mathbf{u}_i^T \mathbf{L}_c^i \mathbf{P}_i + \frac{p}{B_{lim}} (A_i)^{fs} & x_i = 1 \\ 0 & x_i = 0 \end{cases}. \tag{19}$$

The minus sign is introduced when minimization of the objective function is considered in the optimization problem.

This analysis is carried out for each element i in the design domain. For solid elements which are not at the fluid-structure boundary (interface), the pressure transferred by the occupying fluid is null and the term $\mathbf{u}_i^T \mathbf{L}_c^i \mathbf{P}_i$ vanishes. The term for buoyancy in the sensitivities are also only for boundary elements. Although the sensitivities for void elements are computed as zero, the application of a numerical filter scheme smooth the sensitivities over the finite elements and voids nearby regions with high sensitivities can return to solid.

It is also important to note that the new term α_{Bi} is only valid when the inequality constraint g is violated. The first term of α_i is the strain energy of element x_i. The second term is the derivative of the pressure loads at the element level. The elements with the lowest sensitivities can be removed from the domain with a minimum change in the objective function. When g is not violated, the compliance derivatives will provide the gradient information for the optimization procedure. For buoyant structures, the minimum compliance would be obtained with the smallest possible structure without holes, i.e., a structure with a very small B. However, as B decreases, g will be violated and the solid elements at the fluid-structure interfaces will have a high sensitivity number because of the penalty factor p, causing elements to be added in the region of the fluid-structure interfaces so that the volume (and consequently B) of the structural design increases. At this point, only elements in the interior of the structure will be removed, since these elements have lower sensitivities.

4. Optimization procedure

Originally, evolutionary structural optimization (ESO) was based on successive elimination of material from the initial design domain (Xie and Steven 1993). Further improvements to the ESO method were made using a bi-directional algorithm (Querin and Steven 1998).

One of the last major developments in ESO-based methods was the convergent and mesh-independent BESO method proposed by Huang and Xie (2007), which allows material to be simultaneously removed and added in the domain until a volume constraint and convergence criterion are satisfied. In general, these methods can be considered gradient-based methods that rely on design updates and result only in 0/1 solutions during the optimization process.

The proposed methodology described in this article is a hard-kill BESO approach, in which some void elements are substituted by incompressible fluid ones and the loads are generated by imposed pressures in the coupled model.

4.1 *Implementation matters for a BESO-based method*

In order to rank all the elements according to their contribution to the objective function, the sensitivity numbers from Equation 19 are evaluated for each element. Boundary and interior elements are identified by checking their neighbouring elements. A solid element is a boundary element if it has at least one fluid neighbour element and an interior element if it does not have any fluid neighbours. A mesh-independency filter is applied over the whole mesh by averaging each elemental sensitivity number with its neighboring elements. The filter scheme is similar to that described by Sigmund and Peterson (1998). To evaluate the filter weights, nodal sensitivity numbers α_j are calculated by averaging the elemental sensitivity numbers of the jth connected elements. These nodal sensitivity numbers must be converted back into elemental sensitivities by projecting a sub-domain Ψ_i with length scale r_{min} centered on the ith element. All the nodes inside Ψ_i must have their nodal sensitivity numbers averaged back to the ith elemental level as follows:

$$\alpha_i = \frac{\sum_{j=1}^{nod} w(r_{ij})\alpha_j}{\sum_{j=1}^{nod} w(r_{ij})}, \tag{20}$$

where r_{ij} is the distance between the node j and the center of the element i, nod is the

total number of nodes inside the design domain and $w(r_{ij})$ is a weight factor whose value is $r_{min} - r_{ij}$ for nodes inside the sub-domain Ψ_i and 0 for nodes outside the sub-domain. This filter scheme can effectively address mesh-dependency and checkerboard problems. However, the objective function and corresponding topology may not be convergent. To avoid this problem, Huang and Xie (2007) showed that the above sensitivity numbers should be averaged with their previous iteration numbers as follows

$$\alpha_i = \frac{\alpha_i^n + \alpha_i^{n-1}}{2}, \tag{21}$$

where n is the current iteration number. Thus, the updated sensitivity number includes the history of the sensitivity information in the previous iterations (Huang and Xie 2007).

For each iteration, a target volume $V_{n+1} = V_n(1 \pm ER)$ is used, where ER is the evolutionary ratio and n the number of the iteration. ER is the percentage change in the structural volume and causes V_{n+1} to increase or decrease toward the final desired structural volume fraction V_s. When $V_n = V_s$, the equality constraint h is active and the target volume V_{n+1} is kept equal to V_s until the convergence of the algorithm. The target volume V_{n+1} sets the threshold α_{th} of the sensitivity numbers. Solid elements ($x_i = 1$) for which $\alpha_i \leq \alpha_{th}$ are switched to the fluid/void condition ($x_i = 0$). Fluid/void elements ($x_i = 0$) are switched to the solid condition ($x_i = 1$) when $\alpha_i > \alpha_{th}$.

Meanwhile, the volume addition ratio (AR) is restricted to a maximum addition ratio AR_{max}, which specifies the maximum allowable solid volume fraction that can be added per iteration. It plays an important role when the inequality constraint g is violated and solid elements at the interfaces have highly penalized sensitivities. Because of filtering, exterior fluid/void elements close to the interfaces are also given high sensitivities and tend to return to solid condition. The amount of these new solid elements is controlled by the maximum admission ratio AR_{max}. This parameter is usually set with similar values to ER, e.g., between 1% and 5%. If $AR > AR_{max}$, only some of the elements with highest sensitivity numbers are added to set $AR = AR_{max}$. Then, some of the elements with the lowest sensitivity numbers are removed to satisfy the target volume V_{n+1}.

When the variables x_i for an element are equal to zero, a decision must be taken as the element can become a fluid element or a void. If the element has at least one fluid element as neighbor, it must be turned into a fluid element. If the element does not have any fluid neighbors, it must be turned into a void. This procedure is repeated until there are no more changes in the fluid-void regions. Thus, some layers of structural elements near the fluid-structure interface can be replaced by fluid elements, and void elements appear only inside the structural domain, similarly as illustrated in Figure 3.

When the prescribed final volume fraction V_s is reached, the target volume remains constant, i.e., $V_{n+1} = V_n$. The algorithm evolves until a stop criterion with a predefined error tolerance τ is satisfied. Here, the convergence is estimated as

$$\frac{|C_n - C_{n-1}| + |C_{n-1} - C_{n-2}|}{C_n - C_{n-1}} \leq \tau, \tag{22}$$

where C_n is the structural compliance value for the current iteration.

4.2 *The extended fluid-structure BESO method*

The evolutionary procedure for the BESO method presented here for buoyancy module design problems is as follows:

(1) Define the design domain, loads and boundary conditions.

(2) Define the BESO parameters.
(3) Discretize the design domain using a finite element (FE) mesh for the given boundary conditions. Initially, the global fluid-structure stiffness matrix must be assembled uncoupled.
(4) Couple and store a current global matrix $\mathbf{K}_n$ with the coupling matrices according to the current design of the nth iteration and the appropriate boundary conditions. Thus, the current $\mathbf{K}_n$ becomes equivalent to the stiffness matrix from Equation 8.
(5) Perform FE analysis (using Equation 8) on the current design to obtain the displacement and pressure responses.
(6) Calculate the sensitivity numbers according to Equation 19.
(7) Apply the filter scheme. Project the nodal sensitivity numbers on the finite element mesh and smooth the sensitivity numbers for all (fluid, void and solid) elements in the design domain.
(8) Average the sensitivity numbers with their values in the previous iteration $(n-1)$ numbers and then save the resulting sensitivity numbers for the next iteration.
(9) Determine the target structural volume V_{n+1} for the next iteration.
(10) Construct a new fluid-structure design by switching design variables x_i from 1 to 0 and from 0 to 1, tracking the advance of the fluid-void regions.
(11) Remove and/or add the element stiffness matrices from the original uncoupled global matrix $\mathbf{K}_g$ according to the change in the current design.
(12) Repeat steps 2-12 until the stop criterion from Equation 22 is satisfied.

5. Numerical results

5.1 *Test case*

To test the algorithm, a simple square-shaped, buoyant structure was chosen. Figure 4 shows the structure floating in a fluid domain. A quarter of the model was discretized with 11664 finite elements, of which 10000 are solid and 1664 fluid. The solid material used was a polymer with Young's modulus $E = 1.25$ KPa and Poisson's ratio $\nu = 0.37$. The pressure P_0 imposed on the fluid domain was an arbitrary value of 1 Pa. The fluid properties are not taken into account in the static analysis when body forces are neglected.

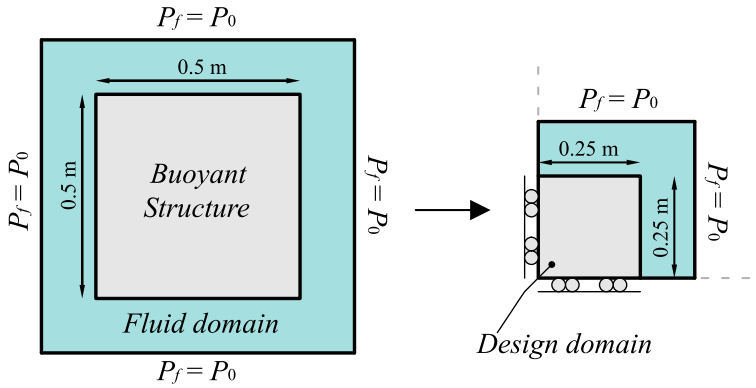

Figure 4.: Design problem: complete fluid-structure model and the design domain used (a quarter of the model) including boundary conditions.

Because of the buoyant nature of the structure, this type of model behaves differently from those used previously in structural topology optimization (Bendsoe and Sigmund

2003; Huang and Xie 2010). A buoyant structure suffers equal compression in all directions, and if it is completely solid, is therefore in a hydrostatic pressure state with the same stress values all over the structural domain independently of the coordinate system. This also implies that the strain energy term $\frac{1}{2}\mathbf{u}_i^T\mathbf{K}_s^i\mathbf{u}_i$ on α_i is equal for all the elements in a structure with no holes inside. Then, starting from a full design domain, the evolutionary topology optimization method would not work without the derivatives $\mathbf{u}_i^T\mathbf{L}_c^i\mathbf{P}_i$ of the design-dependent pressure loads.

The parameters of the BESO method for the test case design problem are set to $ER = 3\%$, $AR_{max} = 5\%$, $V_s = 15\%$ and $\tau = 0.01$. The filter radius applied is $r_{min} = 0.01$ m, the penalty factor is chosen to be a constant $p = 1 \cdot 10^5$ and the buoyancy lower limit B_{lim} is set to 0.0419 m^2, which is equivalent to the area of 6700 elements from the design domain. Figure 5 shows snapshots of the evolutionary topology solution until final convergence. Initially, only solid elements at the fluid-structure interface are removed because of the influence of $\mathbf{u}_i^T\mathbf{L}_c^i\mathbf{P}_i$ on the sensitivities.

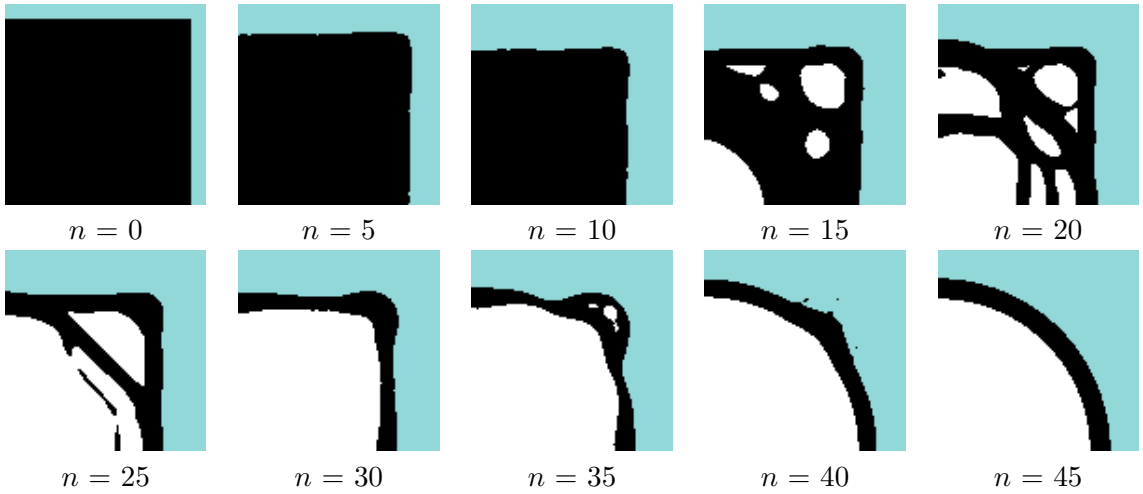

Figure 5.: Snapshots of the test-case solution.

When the buoyancy inequality constraint is violated, the penalty factor p gives the elements at the interface a high sensitivity number. Then, holes are created in the structure and the algorithm evolves until convergence is reached. In Figure 6, it can be seen that the buoyancy area B decreases in the first iterations until the buoyancy inequality constraint is violated (iteration 12) and B increases.

Figure 7 shows the evolutionary history for the global mean compliance of the buoyant structure. It must be pointed out that the strong oscillations on the mean compliance values may be caused by the penalization on g and its consequent change in the joint volume B or by the break of structural members. In Figure 7 the intermediate topologies are detailed for the strong oscillations in the mean compliance convergence curve. In this case, the highest compliance is linked to a topology with a broken structural member. The solution is then said to be convergent with $C = 2.6518{\cdot}10^{-4}$ Nm at the iteration 45 according to the Equation 22, which evaluates two consecutive iterations.

For this simple 2D test case, the final solution obtained was a hollow cylinder. This result is intuitive and was already expected as the optimal buoyant structure with a volume constraint. If one takes the formula for the area of a circle $A_c = 4B = \pi r_c^2$, where r_c is the radius of the circle and the number 4 appears because a quarter of the whole design model was used (see Figure 8), one can predict the radius of the optimal structure

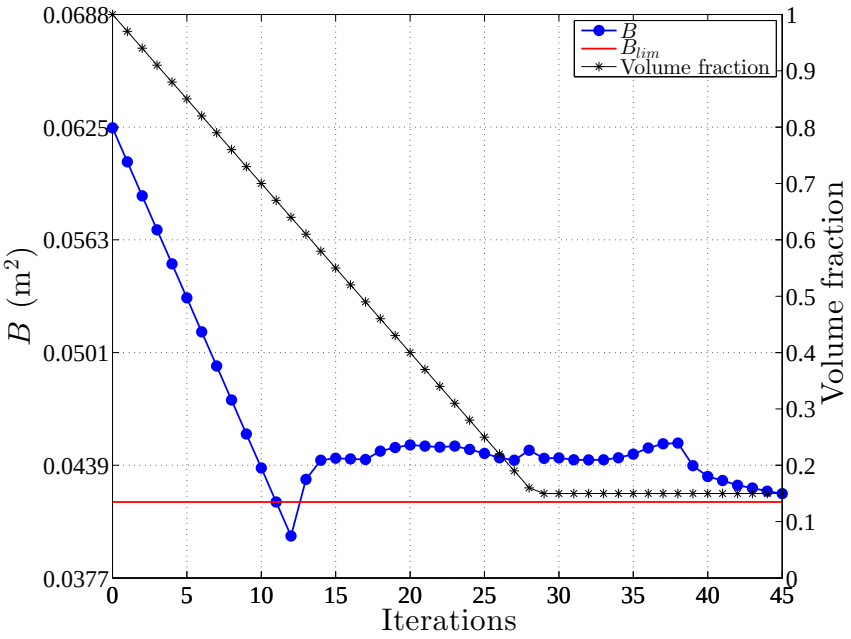

Figure 6.: Evolutionary history of the buoyancy area B of the buoyant structure.

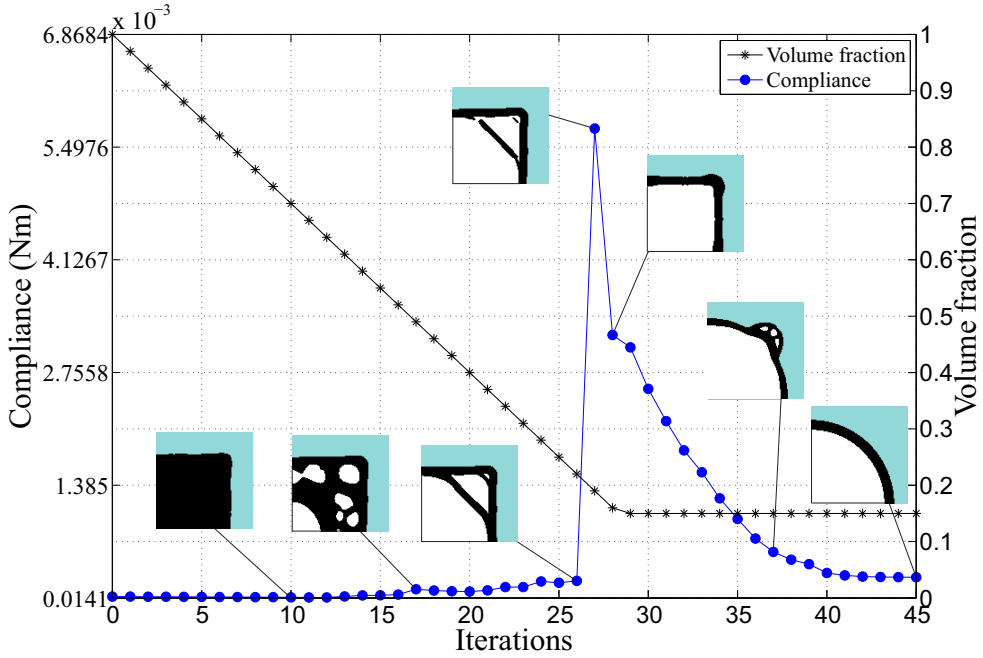

Figure 7.: Evolutionary history of the global mean compliance of the buoyant structure.

for this test case as function of B:

$$r_c = \sqrt{\frac{4B}{\pi}}. \tag{23}$$

The formula of a cross-sectional area A_s of a hollow cylinder with an external radius r_c and internal radius r_i can be given as $4A_s = \pi\left(r_c^2 - r_i^2\right)$. If r_c is substituted and r_i is isolated, one can predict the internal radius for the final optimal hollow cylinder as a

function of A_s,

$$r_i = \sqrt{\frac{4\,(B - A_s)}{\pi}}, \tag{24}$$

and, consequently, the thickness t of the hollow cylinder $t = r_c - r_i$.

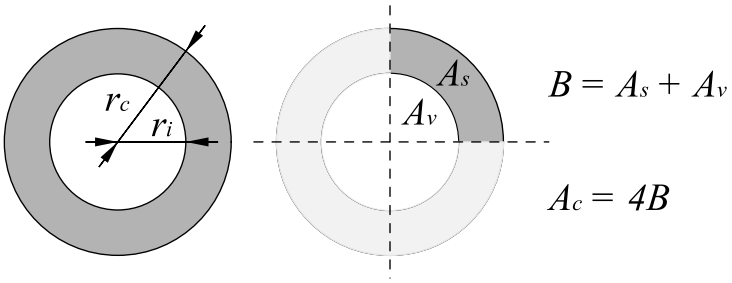

Figure 8.: Geometric properties of the hollow cylinder associated with the solutions for the test case.

In conclusion, for this simple test case r_c depends on B and r_i is directly determined by V_s, since A_s depends on the final volume of solid material. The results of numerical analysis of the previous equations for different hollow cylinders obtained using the BESO method with different values of B_{lim} are shown in Table 1. These examples are obtained with the following optimization parameters: $ER = 5\%$, $AR_{max} = 5\%$, $V_s = 20\%$, $r_{min} = 0.015$ m, $p = 1 \cdot 10^4$, $\tau = 0.001$ and different values for B_{lim}. The differences between the geometrical measurements of the BESO topology solutions and the analytical results of the previous equations are given by the thickness t in Table 1, which is always smaller than the element size (0.0025). Thus, the numerical BESO solutions agree with the analytical equations, validating the methodology. Problems with greater complexity (as in the next example) can be expected to result in more complex designs.

5.2 *Study case*

As a study case, a subsea buoy design problem was chosen. The buoy is built with two semicircles with an inner and outer radius, and the pipeline is attached to the buoy's inner edge. At higher oil temperatures and deepwater pressures, a pipeline's natural tendency is to relieve its axial stress by buckling. The type of buoyancy module described here reduces the severity of buckle bending by using buoyancy to decrease the operational submerged weight of the pipeline, especially in long vertical pipelines such as the catenary riser. In some other applications, e.g., when pipelines are installed over subsea soil, the buoyancy module decreases lateral soil-structure friction using the same buoyancy principle.

For this buoyancy-module problem, only one of the two semicircles making up the design is considered. Figure 9(a) shows the floating structural model immersed in a pressurized fluid domain. Half of the model is discretized with finite elements and used as design domain. The boundary conditions for the finite element model used are shown in Figure 9(b). The inner edge (represented by a thicker line) is considered a non-design domain, i.e., it remains as solid material during the whole algorithm. The inner radius should remain fixed as a design requirement. The solid material adopted is a polymer with Young's modulus $E = 1.25$ kPa and Poisson's ratio $\nu = 0.37$. The pressure P_0 imposed on the fluid domain is an arbitrary value of 1 Pa.

Table 1.: Dimensions of the hollow cylinders identified as the stiffest buoyant structures using the BESO method with different values of B_{lim}. The thickness t obtained with the topology solutions and the analytical values are shown in the columns *BESO* and *Theory*, respectively, as well as the absolute difference between them (column *Diff.*).

Topology	B_{lim} (m^2)	B (m^2)	A_s (m^2)	r_c (m)	r_i (m)	t (m) *BESO*	t (m) *Theory*	%*Diff.*
	0.0288	0.0333	0.0125	0.2050	0.1625	0.0425	0.0431	0.0007
	0.0331	0.0381	0.0125	0.2200	0.1800	0.0400	0.0397	0.0003
	0.0375	0.0429	0.0125	0.2325	0.1975	0.0350	0.0370	0.0020
	0.0419	0.0477	0.0125	0.2450	0.2125	0.0325	0.0347	0.0022

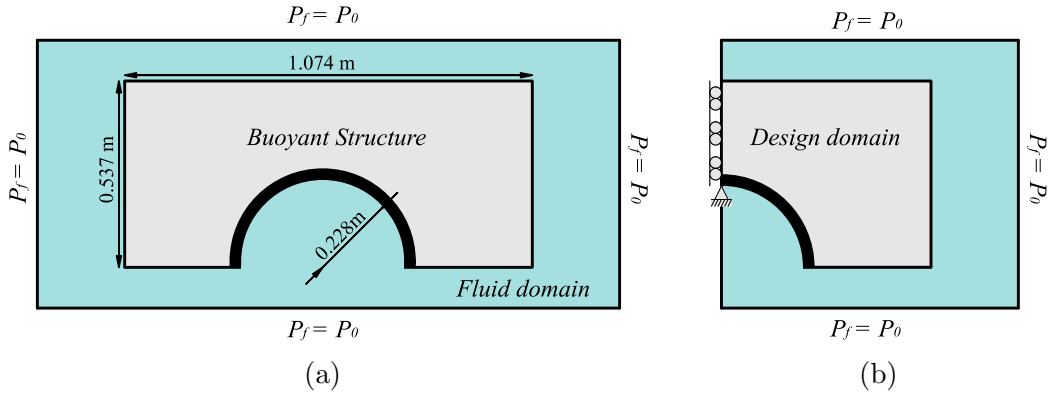

(a) (b)

Figure 9.: Structural optimization design problem: (a) complete fluid-structure model and (b) design domain using half of the model showing the boundary conditions for the structure.

For the design problem shown in Figure 9 two initial solutions are considered, one starting from the initial full design and another with an initial semicircle solution covering 75% of the design domain. The whole model is discretized with 51513 finite elements. The evolutionary ratio (ER) is chosen to be 1%, i.e., the volume of solid material decreases 1% in each iteration until it reaches V_s, which is chosen to be 30%. The other parameters of the BESO method are set as, $AR_{max} = 5\%$, $r_{min} = 0.0125$ m and $\tau = 0.001$. Figure 10 shows the initial solutions and final topologies for both cases, as well as a comparison

case in which the fluid-structure interfaces are kept fixed. The buoyancy area limit B_{lim} is chosen as 0.1485 m^2, which is equivalent to 80% of the area of the initial semicircle solution in Figure 10(b). The penalty factor is chosen as a constant $p = 1 \cdot 10^5$.

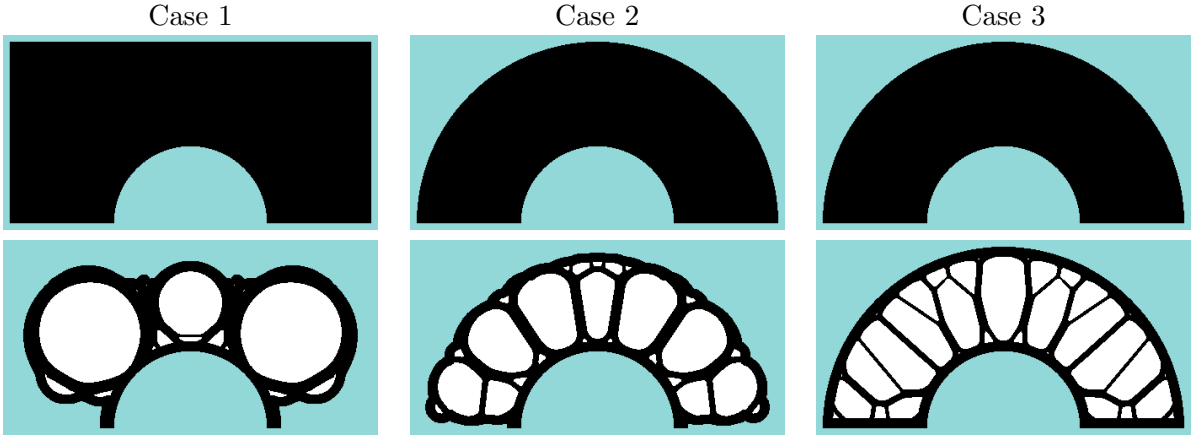

Case 1	Case 2	Case 3
$B = 0.1622$ m^2	$B = 0.1628$ m^2	$B = 0.1856$ m^2
$C = 4.2429{\cdot}10^{-4}$ Nm	$C = 4.2061{\cdot}10^{-4}$ Nm	$C = 5.8800{\cdot}10^{-4}$ Nm
$V_s = 30\%$	$V_s = 30\%$	$V_s = 30\%$

Figure 10.: Buoy module designs with topology optimization: Case 1 - full design domain and final topology; Case 2 - initial semicircle solution and final topology (design-dependent loads); Case 3 - initial semicircle solution and final topology with fixed fluid-structure interfaces (fixed loads).

It can be seen that the final topologies in Case 1 and Case 2 mainly cover the areas in the "initial guess" solutions, indicating that the starting topology exerts a strong influence on the final solution and suggesting that the designer should choose the initial guess according to some desired final solution. This behavior is expected as the structure is floating. When pressure is applied all over a floating structure that can change its shape and topology, the structure starts to seek an equilibrium state, behaving like bubbles. Indeed, the final results in this work are bubble-like structures. This behavior can be observed in Figure 11, which shows snapshots of the solution for Case 2.

Although it uses the same amount of solid material, the structure in Case 2 is the stiffest and represents an increase in stiffness and reduction in buoyancy area compared with Case 3 of around 39% and less than 13%, respectively. The results for Case 1 were very similar to those for Case 2. Figure 12 and 13 show the evolutionary history of the buoyancy area and mean compliance, respectively, for Case 2.

The following analyses show the different solutions obtained using different parameter settings and allow the details of the method to be explored. The reference parameters are the same from Case 2. Figure 14 shows the topologies produced when three different evolutionary ratios were used (1%, 3% and 5%). The numerical results did not vary significantly, and the final solutions differed only in some aspects of their topology, reflecting different local minima.

Another important parameter of the method is the maximum admission ratio AR_{max}, which can limit the amount of added solid elements per iteration. Figure 15 presents different solutions obtained with different AR_{max}'s. It was observed that smaller AR_{max}'s leaded to smaller changes in the fluid-structure boundaries because less solid elements are allowed to be added in these regions per iteration. Higher admission ratios allow more drastic changes in the interface shapes. However, the amount of solid elements is also limited by the filter radius, which extrapolates the highly penalized sensitivities in the interface regions. Thus, the AR_{max} parameter does not affect the solution with a

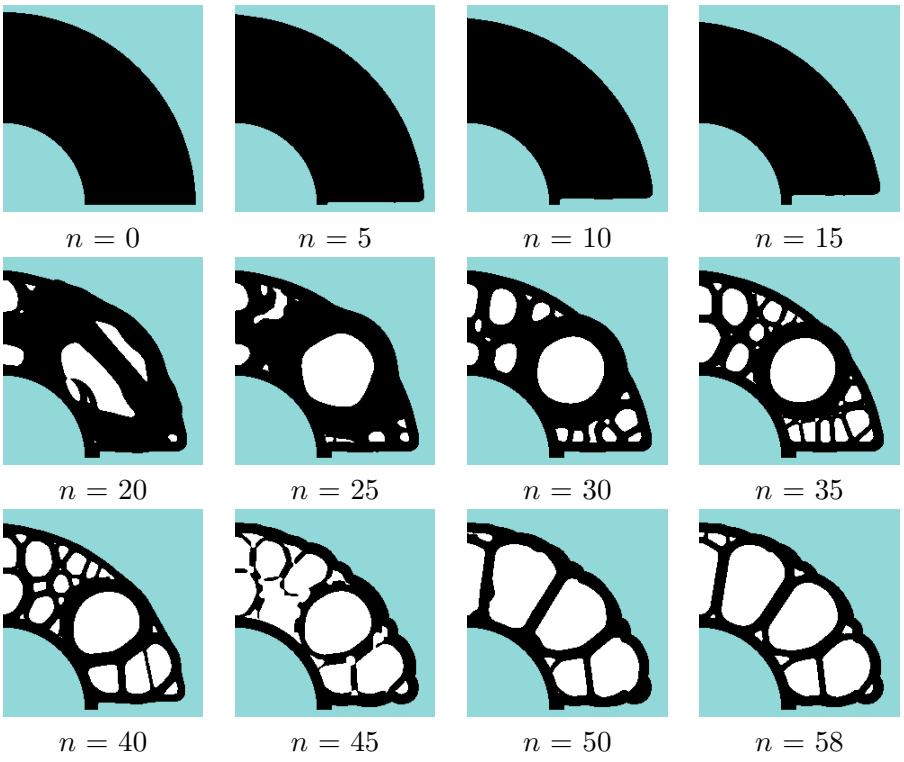

Figure 11.: Snapshots of the Case 2 solution after different iterations.

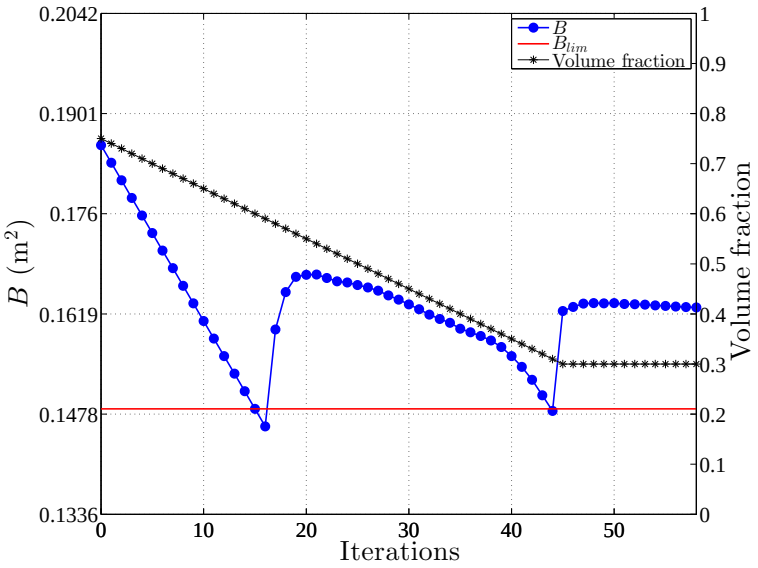

Figure 12.: Evolutionary history of the buoyancy area for Case 2.

high enough value. As seen in Figure 15, the final solution is the same for $AR_{max} = 5\%$ and $AR_{max} = 100\%$, this last being equivalent as not considering the rule of maximum addition ratio.

Figure 16 shows different solutions when the penalty factor p was varied. It can be seen that this variable exerted a considerable influence on the solutions. Smaller penalty factors produced greater variations in the outer shape than higher penalty factors.

A very high penalty factor may result into difficulties in the optimization procedures.

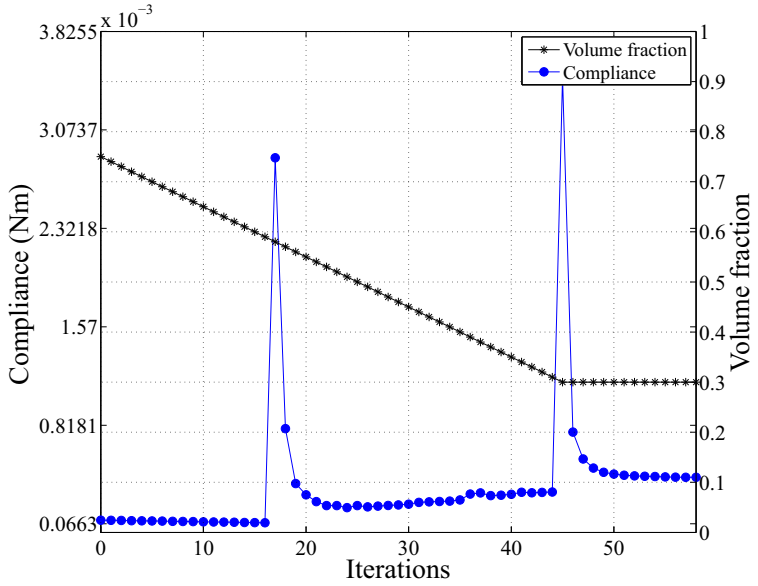

Figure 13.: Evolutionary history of the mean compliance of the buoy in Case 2.

$ER = 1\%$
$C = 4.2061{\cdot}10^{-4}$ Nm
$B = 0.1628$ m^2

$ER = 3\%$
$C = 4.1250{\cdot}10^{-4}$ Nm
$B = 0.1621$ m^2

$ER = 5\%$
$C = 4.1123{\cdot}10^{-4}$ Nm
$B = 0.1619$ m^2

Figure 14.: Different solutions with different evolutionary ratios.

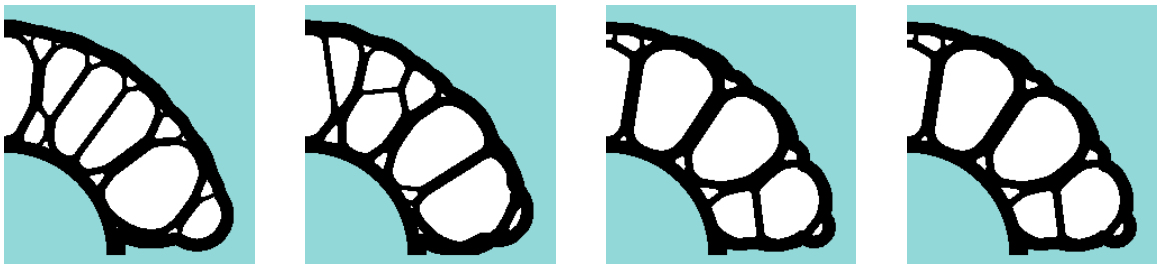

$AR_{max} = 1\%$
$C = 4.2061{\cdot}10^{-4}$ Nm
$B = 0.1628$ m^2

$AR_{max} = 3\%$
$C = 4.1250{\cdot}10^{-4}$ Nm
$B = 0.1621$ m^2

$AR_{max} = 5\%$
$C = 4.1123{\cdot}10^{-4}$ Nm
$B = 0.1619$ m^2

$AR_{max} = 100\%$
$C = 4.1123{\cdot}10^{-4}$ Nm
$B = 0.1619$ m^2

Figure 15.: Different solutions with different maximum admission ratios.

A continuous variation of the penalty factor can be used to try avoiding these issues. Figure 17 presents a solution obtained with penalty variation. The initial penalty factor was chosen to be $p = 5 \cdot 10^2$ and updated with the rule $p^{next} = 10 \cdot p^{current}$ for each iteration the constraint g was active. As presented, the problem shows to have many local minima and the solution is also affected by the penalty update strategy adopted.

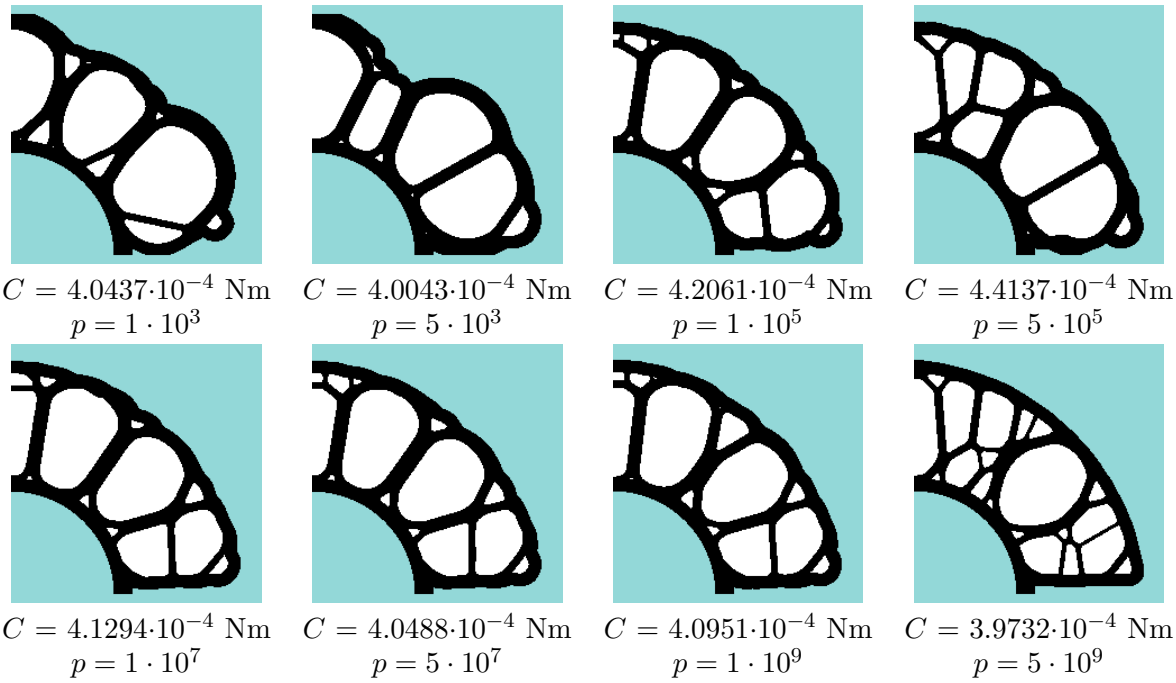

$C = 4.0437{\cdot}10^{-4}$ Nm, $p = 1 \cdot 10^3$ | $C = 4.0043{\cdot}10^{-4}$ Nm, $p = 5 \cdot 10^3$ | $C = 4.2061{\cdot}10^{-4}$ Nm, $p = 1 \cdot 10^5$ | $C = 4.4137{\cdot}10^{-4}$ Nm, $p = 5 \cdot 10^5$

$C = 4.1294{\cdot}10^{-4}$ Nm, $p = 1 \cdot 10^7$ | $C = 4.0488{\cdot}10^{-4}$ Nm, $p = 5 \cdot 10^7$ | $C = 4.0951{\cdot}10^{-4}$ Nm, $p = 1 \cdot 10^9$ | $C = 3.9732{\cdot}10^{-4}$ Nm, $p = 5 \cdot 10^9$

Figure 16.: Different solutions with different penalty factors p.

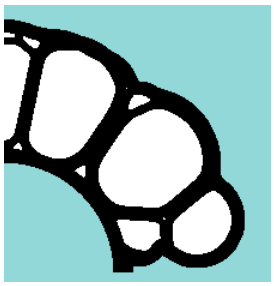

$C = 4.0538{\cdot}10^{-4}$ Nm
$p^{initial} = 5 \cdot 10^2$ and $p^{final} = 5 \cdot 10^5$

Figure 17.: Solution obtained using a continuous variation of the penalty factor.

The strain energy distributions of the final structures for Case 2 (variable boundary with continuous penalty variation) and Case 3 (fixed boundary) for $p = 1 \cdot 10^5$ are shown in Figure 18. Both strain energy distributions are normalized to the maximum strain energy in Case 3 so that the same scale can be used. It can be observed that for the bubble-like structure (Case 2) the strain energy distribution is much smoother than for Case 3, in which the predominant structural patterns are bars under compression. This result is reflected in the compliance value, which is around 45% smaller for the bubble-like design. This justifies the use of the proposed methodology even though the final buoyancy area of the buoy with the variable boundary is smaller than the buoyancy area of the fixed-boundary buoy in this example. One important point worth noting is that the proposed buoy module can be used in a region where drag forces are negligible, i.e., where the loads produced by the subsea fluid flow are much smaller than the deepwater pressure loads. Because its external shape is similar to that of the buoy in Case 3, this solution may also be suitable for use in regions where drag forces are quite high. However, in cases where the solution looks like Case 1, i.e., the buoy has a significantly different shape, further analysis may be needed.

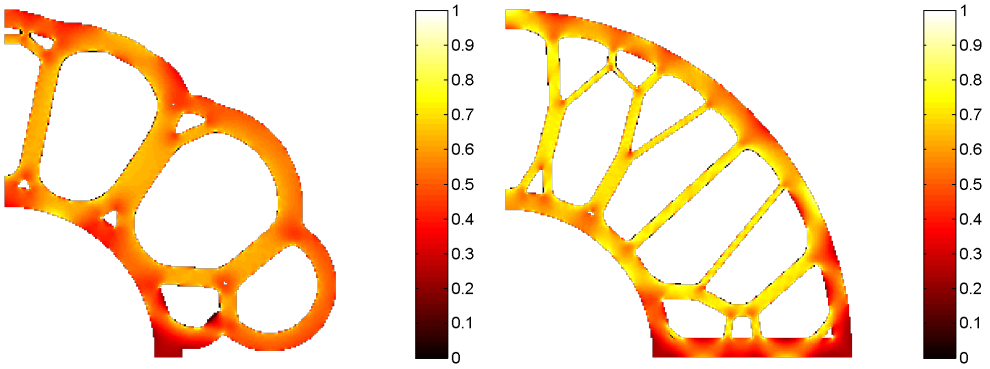

$C = 4.0538{\cdot}10^{-4}$ Nm
$B = 0.1614$ m^2

$C = 5.8800{\cdot}10^{-4}$ Nm
$B = 0.1856$ m^2

Figure 18.: Normalized strain energy distribution for the buoyancy module designed with the proposed methodology using continuous p variation and the case with fixed boundaries.

6. Conclusions

This work proposes the use of topology optimization to identify alternative structural designs in offshore engineering. The specific case of fully submerged buoyancy modules under constant underwater pressure loads is considered. The extended BESO method proposed by Picelli, Vicente and Pavanello (2015) is used to directly circumvent the known issues in topology optimization of design-dependent pressure loading problems. The discrete nature of the evolutionary procedures allows the switch between solids, fluids and voids with explicitly defined fluid-structure interfaces. Thus, no parametrization schemes are needed to model the pressure surfaces. A new inequality constraint is proposed to guarantee minimum required buoyancy effects, measured by the volume of the displaced fluid. It was shown that with a penalty factor, the evolutionary optimization problem could handle a different constraint rather the standard volume one. The final topologies were bubble-like structures, results that confirms the effectiveness of the proposed methodology. The parameters of the method were discussed. Comparison of the results with a case in which the pressure loads are fixed showed that a stiffer structure could be designed by moving the fluid-structure interfaces and fulfilling the buoyancy requirements simultaneously. If other types of forces are negligible, e.g., viscous flow loads, the proposed solutions can be used as a starting point for the design of new deepwater buoyancy modules to support oil pipelines. Further improvements can be carried out, such as the consideration of non-constant pressure fields or buckling constraints.

Acknowledgements

This work was supported by the São Paulo Research Foundation (FAPESP) [2011/09730-6, 2013/08293-7, 2013/00085-6].

References

Axisa, Franois and Antunes, Jos. 2007. *Modelling of Mechanical Systems: Fluid-Structure Interaction*. Oxford, UK: Butterworth-Heinemann.

Bendsoe, M. P. and Kikuchi, N. 1988. “Generating optimal topologies in structural design using

a homogenization method." *Computer Methods in Applied Mechanics and Engineering* 71: 197–224.

Bendsoe, Martin Philip and Sigmund, Ole. 2003. *Topology Optimization - Theory, Methods and Applications*. 2nd ed. Berlin: Springer.

Bourdin, B. and Chambolle, A. 2003. "Design-dependent loads in topology optimization" *ESAIM: Control, Optimisation and Calculus of Variations* 9: 19–48.

Bruggi, M. and Cinquini, C. 2009. "An alternative truly-mixed formulation to solve pressure load problems in topology optimization" *Computer Methods in Applied Mechanics and Engineering* 198: 1500–1512.

Clausen, A., Aage, N. and Sigmund, O. 2014. "Topology optimization with flexible void area" *To appear in Structural and Multidisciplinary Optimization*.

Chen, B., Silva, E. C. N. and Kikuchi, N. 2001. "Advances in computation design and optimization with application to MEMS." *International Journal for Numerical Methods In Engineering* 52: 23–62.

Deaton, J. D. and Grandhi, R. V. 2014. "A survey of structural and multidisciplinary continuum topology optimization: post 2000" *Structural and Multidisciplinary Optimization* 49: 1–38.

Du, J. and Olhoff, N. 2000. "Topological optimization of continuum structures with design-dependent surface loading Part I: new computational approach for 2D problems" *Structural and Multidisciplinary Optimization* 27: 151–165.

Duhring, M. B., Jensen, J. S. and Sigmund, O. 2008. "Acoustic design by topology optimization" *Journal of Sound and Vibration* 317: 557–575.

Hammer, V. B. and Olhoff, N. 2000. "Topology optimization of continuum structures subjected to pressure loading" *Structural and Multidisciplinary Optimization* 19: 85–92.

Huang, X. and Xie, Y. M. 2007. "Convergent and mesh-independent solutions for the bi-directional evolutionary structural optimization method" *Finite Elements in Analysis and Design* 43: 1039–1049.

Huang, X. and Xie, Y. M. 2009. "Bi-directional evolutionary topology optimization of continuum structures with one or multiple materials" *Computational Mechanics* 43: 393–401.

Huang, X. and Xie, Y. M. 2010a. "A further review of ESO type methods for topology optimization" *Structural and Multidisciplinary Optimization* 41: 671–683.

Huang, Xiaodong and Xie, Mike, 2010. *Evolutionary topology optimization of continuum structures: methods and applications*. Chichester: Wiley.

Huang, X., Zhou, S., Sun, G., Li, G. and Xie, Y. M. 2015. "Topology optimization for microstructures of viscoelastic composite materials" *Computer Methods in Applied Mechanics and Engineering* 283: 503–516.

Lee, E. and Martins, J. R. R. A. 2012. "Structural topology optimization with design-dependent pressure loads" *Computer Methods in Applied Mechanics and Engineering* 233: 40–48.

Luenberger, David G. and Ye, Yinyu. 2008. *Linear and Nonlinear Programming*. Springer; 3rd edition.

Luo, Z., Zhang, N., Ji, J. and Wu, T. 2012. "A meshfree level-set method for topological shape optimization of compliant multiphysics actuators" *Computer Methods in Applied Mechanics and Engineering* 223–224: 133–152.

Morand, Henri J. P. and Ohayon, Roger. 1995. *Fluid Structure Interaction - Applied Numerical Methods*. Masson, Paris: John Wiley & Sons, Inc.

Picelli, Renato. 2015. "Evolutionary Topology Optimization of Fluid-structure Interaction Problems." PhD diss., University of Campinas.

Picelli, R., Vicente, W. M. and Pavanello, R. 2015. "Bi-directional evolutionary structural optimization for design-dependent fluid pressure loading problems" *Engineering Optimization* 47: 1324–1342.

Picelli, R., Vicente, W. M., Pavanello, R. and Xie, Y. M. 2015. "Evolutionary topology optimization for natural frequency maximization considering acoustic-structure interaction" *Finite Elements in Analysis and Design* 106: 56–64.

Picelli, R., Vicente, W. M., Pavanello, R. and van Keulen, F. 2015. "Topology optimization considering design-dependent Stokes flow loads" In: *Proceedings of the 11th World Congress of Structural and Multidisciplinary Optimization (WCSMO-11)*, Sydney, Australia.

Querin, O. M. and Steven, G. P. 1998. "Evolutionary structural optimisation (ESO) using a

bidirectional algorithm" *Engineering Computations* 15: 1031–1048.

Saito, D., Cordeiro, L. R. S., Castro, F. A., Medeiros, C. J. and Ribeiro, G. D. 2011. "Innovative supports of risers and corresponding installation procedures" In: *ASME Proceedings of the 30th International Conference on Ocean, Offshore and Arctic Engineering*, Volume 4: Pipeline and Riser Technology, Rotterdam, The Netherlands.

Shu, L., Wang, M. Y. and Ma, Z. 2014. "Level set based topology optimization of vibrating structures for coupled acoustic-structure dynamics" *Computers and Structures* 132: 34–42.

Sigmund, O. and Peterson, J. 1998. "Numerical instabilities in topology optimization: A survey on procedures dealing with checkerboards, mesh-dependencies and local minima" *Structural Optimization* 16: 68–75.

Sigmund, O. and Clausen, P. M. 2007. "Topology optimization using a mixed formulation: An alternative way to solve pressure load problems" *Computer Methods in Applied Mechanics and Engineering* 196: 1874–1889.

Silva, F. I. and Pavanello, R. 2010. "Synthesis of porous-acoustic absorbing systems by an evolutionary optimization method" *Engineering Optimization* 42 (10): 887–905.

van Dijk, N. P., Maute, K., Langelaar, M. and van Keulen, F. 2013. "Level-set methods for structural topology optimization: a review" *Structural and Multidisciplinary Optimization* 48: 437–472.

Vicente, W. M., Picelli, R., Pavanello, R. and Xie, Y. M. 2015. "Topology optimization of frequency responses of fluid-structure interaction systems" *Finite Elements in Analysis and Design* 98: 1–13.

Vicente, W. M., Zhihao, Z., Pavanello, R., Calixto, T. K. L., Picelli, R., and Xie, Y. M. 2015. "Concurrent topology optimization for minimizing frequency responses of two-level hierarchical structures" *Computer Methods in Applied Mechanics and Engineering* 301: 116–136.

Xia, L. and Breitkopf, P. 2014. "Concurrent topology optimization desin of material and structure within FE^2 nonlinear multiscale analysis framework" *Computer Methods in Applied Mechanics and Engineering* 278: 524–542.

Xia, L. and Breitkopf, P. 2015. "Multiscale structural topology optimization with an approximate constitutive model for local material microstructure" *Computer Methods in Applied Mechanics and Engineering* 286: 147–167.

Xia, Q., Wang, M. Y. and Shi, T. 2015. "Topology optimization with pressure load through a level set method" *Computer Methods in Applied Mechanics and Engineering* 283: 177–195.

Xie, Y. M. and Steven, G. P. 1993. "A simple evolutionary procedure for structural optimization" *Computers and Structures* 49: 885–896.

Yoon, G. H., Jensen J. S. and Sigmund, O. 2007. "Topology optimization of acoustic-structure interaction problems using a mixed finite element formulation" *International Journal for Numerical Methods in Engineering* 70: 1049–1075.

Yoon, G. H. and Sigmund, O. 2008. "A monolithic approach for topology optimization of electrostatically actuated devices" *Computer Methods in Applied Mechanics and Engineering* 197: 4062–4075.

Yoon, G. H. 2010. "Topology optimization for stationary fluid-structure interaction problems using a new monolithic formulation" *International Journal for Numerical Methods in Engineering* 82: 591–616.

Zhang, H., Liu, S. and Zhang, X. 2010. "Topology optimization of 3D structures with design-dependent loads" *Acta Mechanica Sinica* 26: 767–775.

Zheng, B., Chang, C. and Gea, H. C. 2009. "Topology optimization with design-dependent pressure loading" *Structural and Multidisciplinary Optimization* 38: 535–543.

Zienkiewicz, O. C. and Bettess, P. 1978. "Fluid-structure dynamic interaction and wave forces. An introduction to numerical treatment" *International Journal for Numerical Methods In Engineering* 13: 1–16.

Zuo, Z. H., Xie, Y. M. and Huang, X. 2010. "An improved bi-directional evolutionary topology optimization method for frequencies" *International Journal of Structural Stability and Dynamics* 10: 55–75.

Zuo, Z. H., Huang, X., Rong, J. H. and Xie, Y. M. 2013. "Multi-scale design of composite materials and structures for maximum natural frequencies" *Materials and Design* 51: 1023–1034.